

# Crystal and Electronic Structures of Conductive Anion-Radical Salts, (2,5-R<sub>1</sub>,R<sub>2</sub>-DCNQI)<sub>2</sub>Cu (DCNQI = N,N'-Dicyanoquinonediimine; R<sub>1</sub>, R<sub>2</sub> = CH<sub>3</sub>, CH<sub>3</sub>O, Cl, Br)

Reizo Kato,<sup>1a</sup> Hayao Kobayashi,<sup>\*,1a</sup> and Akiko Kobayashi<sup>1b</sup>

Contribution from the Department of Chemistry, Faculty of Science, Toho University, Funabashi, Chiba, 274, Japan, and Department of Chemistry, Faculty of Science, The University of Tokyo, Hongo, Bunkyo-ku, Tokyo, 113, Japan. Received August 29, 1988

**Abstract:** Crystal structures of a series of highly conductive anion-radical salts with formula (2,5-R<sub>1</sub>,R<sub>2</sub>-DCNQI)<sub>2</sub>Cu (DCNQI = N,N'-dicyanoquinonediimine; R<sub>1</sub>, R<sub>2</sub> = CH<sub>3</sub>, CH<sub>3</sub>O, Cl, Br) have been studied at room temperature and 100 K. At room temperature, all these compounds are isostructural (tetragonal, space group *I*<sub>4</sub>/a). The structure consists of a face-to-face DCNQI column along the crystallographic *c* axis. The Cu cation is coordinated in *D*<sub>2d</sub> distorted tetrahedral fashion to the N atoms of the DCNQI molecules. The metal-insulator transition in this system is attended by an abrupt contraction of the *c* axis. The X-ray satellite reflections that indicate the periodic lattice distortion with a period of 3*c* appear below the metal-insulator transition temperature (*T*<sub>M-1</sub>). The superstructure wave vector (0,0,*c*\*/3) suggests the mixed-valence state of Cu (Cu<sup>+</sup>:Cu<sup>2+</sup> = 2:1). The enhancement of the *D*<sub>2d</sub> distortion of the coordination tetrahedron occurs intensively at *T*<sub>M-1</sub>. The electronic structure of this system was investigated by the simple tight-binding band calculations. The essential point is that the mixed-valence state of Cu leads to the mixing of the organic 2*p*π orbitals and d orbitals. This is responsible for the "multi-Fermi surface" nature of this system that contains more than two pairs of planelike surface in such a way that no single modulation wave vector can produce a gap all over the Fermi surfaces. This is a new strategy for the suppression of the metal-insulator transition in the molecular conductor. The intensive deformation of the coordination tetrahedron at *T*<sub>M-1</sub> expands the ligand field splitting and stabilizes the lower d orbitals of Cu. This decreases the number of the d orbitals participating in the *p*π-d mixing and weakens the multi-Fermi surface nature, which leads to the gap formation by the charge density wave (CDW). Therefore, the metal-insulator transition of this system is considered to be a cooperative structural-phase transition induced by the deformation of the coordination tetrahedron around Cu and the CDW formation of the DCNQI column.

There has been remarkable progress in the field of molecular materials with special properties, such as superconductivity. The conducting system based on planar π-conjugated molecules, for example TTF-TCNQ, prefers highly anisotropic molecular arrangement (column structure) and one-dimensional electronic structure. The typical one-dimensional metal whose Fermi surface contains a pair of flat and parallel sheets easily undergoes a metal-insulator transition caused by CDW (charge density wave) or SDW (spin density wave) formation at low temperature. In this case, a periodic modulation of potential represented by a single wave vector produces a gap over the whole Fermi surface. In the course of the development of the molecular superconductor, it has been the key step to overcome such "Fermi surface instability". The importance of two-dimensionality characterized by a cylindrical Fermi surface has been demonstrated by three types of ambient-pressure superconductors, β-, θ-, and κ-(BEDT-TTF)<sub>2</sub>I<sub>3</sub> (BEDT-TTF = bis(ethylenedithio)tetrathiafulvalene).<sup>2</sup> The crystal structures of these superconductors are characterized by the extended two-dimensional molecular arrangements of BEDT-TTF molecules. Recently, κ-(BEDT-TTF)<sub>2</sub>Cu(NCS)<sub>2</sub>, which contains the κ-type molecular arrangement, has exhibited superconducting transition at higher than 10 K (*T*<sub>c</sub> = 10.4 K).<sup>3</sup> In the field of the molecular superconductor, it has become a promising strategy to consider the conditions under which the two-dimensional electronic structure is constructed.

On the other hand, in the course of studies on the electronic structure of two superconducting Ni(dmit)<sub>2</sub>(dmit = 4,5-dimercapto-1,3-dithiole-2-thione) salts (TTF-[Ni(dmit)<sub>2</sub>]<sub>2</sub>)<sup>4</sup> and

Me<sub>4</sub>N[Ni(dmit)<sub>2</sub>]<sub>2</sub><sup>5</sup>, we have noticed that intermolecular interactions among the conduction molecular orbitals [the highest occupied molecular orbital (HOMO) of the donor and the lowest unoccupied molecular orbital (LUMO) of the acceptor] in these compounds have rather strong one-dimensional character. These compounds, however, show neither CDW nor SDW formation. We have proposed a "multi-Fermi surface" model for an origin of the stable metallic state of these Ni(dmit)<sub>2</sub>-based molecular metals.<sup>6</sup> The Fermi surface of the typical multi-Fermi surface system contains more than two pairs of sheets in such a way that no single modulation wave can produce a gap all over the Fermi surface. In such a system, a complete gap formation requires a complex perturbation potential, which is no longer so energetically favorable compared with the purely one-dimensional case. This idea of the multi-Fermi surface system has opened a new way to the molecular superconductor based on the column structure.

With these guiding principles in mind, we have started a search for new types of molecular materials based on the π acceptor DCNQI (DCNQI = N,N'-dicyanoquinonediimine). Our interest in the above system was initiated by the appealing structural feature of (2,5-DMe-DCNQI)<sub>2</sub>Cu (2,5-DMe-DCNQI = 2,5-dimethyl-N,N'-dicyanoquinonediimine) reported by Aumüller et al. in 1986.<sup>7</sup> This compound remains highly conductive down to 1.3 K with no metal-insulator transition. In the crystal of this com-

(4) (a) Bousseau, M.; Valade, L.; Legros, J.-P.; Cassoux, P.; Garbouskas, M.; Interrante, L. V. *J. Am. Chem. Soc.* **1986**, *108*, 1908-1916. (b) Brossard, L.; Ribault, M.; Bousseau, M.; Valade, L.; Cassoux, P. *C. R. Acad. Sci., Ser.* **2** **1986**, *302*, 205-210. (c) Brossard, L.; Ribault, M.; Valade, L.; Cassoux, P. *Physica B+C (Amsterdam)* **1986**, *143B*, 378-380.

(5) (a) Kim, H.; Kobayashi, A.; Sasaki, Y.; Kato, R.; Kobayashi, H. *Chem. Lett.* **1987**, 1799-1802. (b) Kobayashi, A.; Kim, H.; Sasaki, Y.; Kato, R.; Kobayashi, H.; Moriyama, S.; Nishio, Y.; Kajita, K.; Sasaki, W. *Chem. Lett.* **1987**, 1819-1822. (c) Kajita, K.; Nishio, Y.; Moriyama, S.; Kato, R.; Kobayashi, H.; Sasaki, W.; Kobayashi, A.; Kim, H.; Sasaki, Y. *Solid State Commun.* **1988**, *65*, 361-363. (d) Kobayashi, A.; Kim, H.; Sasaki, Y.; Moriyama, S.; Nishio, Y.; Kajita, K.; Sasaki, W.; Kato, R.; Kobayashi, H. *Synth. Met.* **1988**, *27*, B339-B346.

(6) Kobayashi, A.; Kim, H.; Sasaki, Y.; Kato, R.; Kobayashi, H. *Solid State Commun.* **1987**, *62*, 57-64.

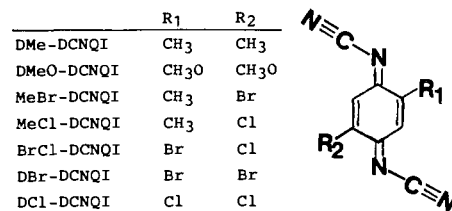
(7) Aumüller, A.; Erk, P.; Klebe, G.; Hünig, S.; von Schütz, J. U.; Werner, H.-P. *Angew. Chem., Int. Ed. Engl.* **1986**, *25*, 740-741.

(1) (a) Toho University. (b) The University of Tokyo.  
 (2) (a) Mori, T.; Kobayashi, A.; Sasaki, Y.; Kobayashi, H.; Saito, G.; Inokuchi, H. *Chem. Lett.* **1984**, 957-960. (b) Kobayashi, H.; Kato, R.; Kobayashi, A. *Synth. Met.* **1987**, *19*, 623-628. (c) Kobayashi, H.; Kato, R.; Kobayashi, A.; Nishio, Y.; Kajita, K.; Sasaki, W. *Chem. Lett.* **1986**, 833-836. (d) Kobayashi, A.; Kato, R.; Kobayashi, H.; Moriyama, S.; Nishio, Y.; Kajita, K.; Sasaki, W. *Chem. Lett.* **1987**, 459-462. (e) Kobayashi, H.; Kato, R.; Nishio, Y.; Kajita, K.; Sasaki, W.; Kobayashi, A.; Mori, T.; Inokuchi, H. *Synth. Met.* **1988**, *27*, A289-A297.  
 (3) Urayama, H.; Yamochi, H.; Saito, G.; Nozawa, K.; Sugano, T.; Kinoshita, M.; Sato, S.; Oshima, K.; Kawamoto, A.; Tanaka, J. *Chem. Lett.* **1988**, 55-58.

Table I. Summary of Crystal Data (at Room Temperature)

compound	(DMe-DCNQI) <sub>2</sub> Cu	(DMeO-DCNQI) <sub>2</sub> Cu	(MeBr-DCNQI) <sub>2</sub> Cu	(MeCl-DCNQI) <sub>2</sub> Cu	(DBr-DCNQI) <sub>2</sub> Cu	(BrCl-DCNQI) <sub>2</sub> Cu	(DCI-DCNQI) <sub>2</sub> Cu
formula	C <sub>20</sub> H <sub>16</sub> N <sub>8</sub> Cu	C <sub>20</sub> H <sub>16</sub> N <sub>8</sub> O <sub>2</sub> Cu	C <sub>18</sub> H <sub>10</sub> N <sub>8</sub> Br <sub>2</sub> Cu	C <sub>18</sub> H <sub>10</sub> N <sub>8</sub> Cl <sub>2</sub> Cu	C <sub>16</sub> H <sub>4</sub> N <sub>8</sub> Br <sub>4</sub> Cu	C <sub>16</sub> H <sub>4</sub> N <sub>8</sub> Br <sub>2</sub> Cl <sub>2</sub> Cu	C <sub>16</sub> H <sub>4</sub> N <sub>8</sub> Cl <sub>4</sub> Cu
formula wt	431.95	463.95	561.70	472.79	691.45	602.52	513.63
crystal dimens, mm	0.18 × 0.22 × 0.35	0.05 × 0.10 × 0.35	0.15 × 0.15 × 0.20	0.15 × 0.20 × 0.33	0.05 × 0.08 × 0.15	0.04 × 0.06 × 0.25	0.03 × 0.05 × 0.35
space group	<i>I</i> 4 <sub>1</sub> /a	<i>I</i> 4 <sub>1</sub> /a	<i>I</i> 4 <sub>1</sub> /a	<i>I</i> 4 <sub>1</sub> /a	<i>I</i> 4 <sub>1</sub> /a	<i>I</i> 4 <sub>1</sub> /a	<i>I</i> 4 <sub>1</sub> /a
cell dimens							
<i>a</i> , Å	21.548 (5)	22.442 (11)	21.601 (6)	21.559 (7)	21.558 (10)	21.569 (11)	21.55 (2)
<i>c</i> , Å	3.871 (1)	3.839 (1)	3.856 (1)	3.823 (2)	3.896 (1)	3.845 (1)	3.816 (1)
<i>V</i> , Å <sup>3</sup>	1797.4	1933.5	1799.2	1776.9	1810.7	1788.8	1772.8
<i>Z</i>	4	4	4	4	4	4	4
<i>d</i> <sub>calc</sub> , g/cm <sup>3</sup>	1.596	1.594	2.074	1.767	2.537	2.237	1.925
linear absorpn coeff, cm <sup>-1</sup>	12.41	11.66	56.41	15.58	99.78	59.74	18.66
scan width (Δω), deg	1.20 + 0.5 tan θ	1.08 + 0.5 tan θ	1.05 + 0.5 tan θ	1.04 + 0.5 tan θ	1.18 + 0.5 tan θ	1.16 + 0.5 tan θ	1.67 + 0.5 tan θ
scan speed, deg/min	4.0	4.0	4.0	4.0	4.0	4.0	4.0
2θ range, deg	0-60	0-60	0-60	0-60	0-60	0-60	0-60
total no. of obsd reflns	1580	1707	1544	1574	1596	1570	1568
no. of unique data with   <i>F</i> <sub>o</sub>   > 3σ( <i>F</i> <sub>o</sub> )	807	655	561	800	704	745	856
weighting scheme <sup>a</sup>	<i>b</i> = 0.01	<i>b</i> = 0.01	<i>b</i> = 0.01	<i>b</i> = 0.01	<i>b</i> = 0.003	<i>b</i> = 0.1	<i>b</i> = 0.01
<i>R</i>	0.0627	0.0535	0.0467	0.0669	0.0415	0.0965	0.0692
<i>R</i> <sub>w</sub>	0.0829	0.0797	0.0818	0.0878	0.0582	0.0965	0.0985

$$^a w = 1/(10.0 + b|F_o|^2) / (|F_o| < 15.0), w = 1/(\sigma^2(F_o) + b|F_o|^2) / (|F_o| \geq 15.0).$$

Figure 1. Molecular structures and their abbreviations of the 2,5-R<sub>1</sub>,R<sub>2</sub>-DCNQI molecules.Table II. Fractional Coordinates and Equivalent Isotropic Thermal Parameters for (DMe-DCNQI)<sub>2</sub>Cu (Room-Temperature Structure)

atom	<i>x</i>	<i>y</i>	<i>z</i>	<i>B</i> <sub>eq</sub> , Å <sup>2</sup>
Cu	0	0.25	0.125	1.7
N(1)	0.4269 (2)	0.2853 (2)	-0.3873 (11)	2.3
N(2)	0.3274 (2)	0.3217 (2)	-0.1461 (11)	2.2
C(1)	0.2902 (2)	0.2859 (2)	0.0477 (11)	1.5
C(2)	0.3051 (2)	0.2227 (2)	0.1376 (13)	1.8
C(3)	0.2664 (2)	0.1874 (2)	0.3289 (11)	1.7
C(4)	0.2819 (2)	0.1210 (2)	0.4195 (13)	2.4
C(5)	0.3796 (2)	0.2991 (2)	-0.2666 (13)	1.6
H(1)	0.342 (2)	0.207 (2)	0.045 (15)	2.0
N(2)	0.311 (3)	0.103 (3)	0.276 (17)	2.9
H(3)	0.251 (3)	0.092 (3)	0.365 (15)	2.9
H(4)	0.293 (3)	0.116 (3)	0.629 (16)	2.9

Table III. Fractional Coordinates and Equivalent Isotropic Thermal Parameters for (DMeO-DCNQI)<sub>2</sub>Cu (Room-Temperature Structure)

atom	<i>x</i>	<i>y</i>	<i>z</i>	<i>B</i> <sub>eq</sub> , Å <sup>2</sup>
Cu	0	0.25	0.125	1.7
N(1)	0.4249 (2)	0.2742 (2)	-0.3898 (16)	2.3
N(2)	0.3307 (2)	0.3119 (2)	-0.1451 (15)	1.9
C(1)	0.2930 (2)	0.2795 (2)	0.0464 (15)	1.6
C(2)	0.3021 (2)	0.2196 (2)	0.1467 (18)	1.6
C(3)	0.2608 (2)	0.1905 (2)	0.3387 (17)	1.6
C(4)	0.3805 (3)	0.2881 (3)	-0.2647 (16)	1.8
CM	0.3155 (3)	0.1002 (3)	0.3224 (19)	2.7
O	0.2653 (2)	0.1333 (2)	0.4457 (13)	2.1
H(1)	0.336 (3)	0.197 (3)	0.059 (18)	2.0
H(2)	0.309 (3)	0.061 (3)	0.420 (19)	2.0
H(3)	0.351 (3)	0.118 (3)	0.439 (18)	2.0
H(4)	0.318 (3)	0.096 (3)	0.075 (18)	2.0

pound 2,5-DMe-DCNQI molecules form the one-dimensional columns, which are connected to one another by tetrahedrally coordinated Cu cations. This structural feature introduces a new concept into the packing motif of the molecular conductor. An interaction between  $\pi\pi$  orbital in the organic molecule and d orbital in the metal ion through the coordination bond would provide electrically and magnetically new types of molecular materials. We report here crystal and electronic structures of anion-radical salts (2,5-R<sub>1</sub>,R<sub>2</sub>-DCNQI)<sub>2</sub>Cu (R<sub>1</sub>, R<sub>2</sub> = Me, MeO, Cl, Br; Figure 1) with relation to their physical properties. In the case of R<sub>1</sub> = R<sub>2</sub> = Me, MeO, a stable metallic behavior was observed down to 0.5 K,<sup>8</sup> and a novel pressure-induced metal-insulator transition was observed.<sup>9</sup> The other DCNQI salts exhibited the cooperative structural-phase transition induced by the intensive deformation of the coordination tetrahedron around Cu and the CDW instability of the DCNQI column.<sup>10</sup> The mixed-valence state of Cu

(8) (a) Kobayashi, H.; Kato, R.; Kobayashi, A.; Mori, T.; Inokuchi, H. *Solid State Commun.* **1988**, *65*, 1351-1354. (b) Hünig, S.; Aumüller, A.; Erk, P.; Meixner, H.; von Schütz, J. U.; Gross, H.-J.; Langohr, U.; Werner, H.-P.; Wolf, H. C.; Burschka, Ch.; Klebe, G.; Peters, K.; Schnering, H. G. *Synth. Met.* **1988**, *27*, B181-B188. (c) Kobayashi, A.; Mori, T.; Inokuchi, H.; Kato, R.; Kobayashi, H. *Synth. Met.* **1988**, *27*, B275-B280.

(9) (a) Mori, T.; Imaeda, K.; Kato, R.; Kobayashi, A.; Kobayashi, H.; Inokuchi, H. *J. Phys. Soc. Jpn.* **1987**, *56*, 3429-3431. (b) Tomic, S.; Jerome, D.; Aumüller, A.; Erk, P.; Hünig, S.; von Schütz, J. U. *Europhys. Lett.* **1988**, *5*, 553-558. (c) Tomic, S.; Jerome, D.; Aumüller, A.; Erk, P.; Hünig, S.; von Schütz, J. U. *J. Phys. C* **1988**, *21*, L203-L207. (d) Tomic, S.; Jerome, D.; Aumüller, A.; Erk, P.; Hünig, S.; von Schütz, J. U. *Synth. Met.* **1988**, *27*, B281-B288.

(10) Kobayashi, A.; Kato, R.; Kobayashi, H.; Mori, T.; Inokuchi, H. *Solid State Commun.* **1987**, *64*, 45-51.

**Table IV.** Fractional Coordinates and Equivalent Isotropic Thermal Parameters for (MeBr-DCNQI)<sub>2</sub>Cu (Room-Temperature Structure)

atom	x	y	z	$B_{\text{eq}}, \text{\AA}^2$
Cu	0	0.25	0.125	1.9
N(1)	0.4270 (1)	0.2860 (1)	-0.3893 (9)	2.4
N(2)	0.3271 (1)	0.3202 (1)	-0.1557 (9)	2.2
C(1)	0.2908 (1)	0.2852 (2)	0.0414 (9)	1.9
C(2)	0.3052 (1)	0.2232 (2)	0.1420 (9)	2.0
C(3)	0.2670 (1)	0.1887 (2)	0.3370 (9)	1.9
MR	0.2875 (0)	0.1098 (0)	0.4532 (2)	2.9
C(5)	0.3790 (1)	0.2986 (1)	-0.2725 (9)	2.0
H(1)	0.334 (2)	0.195 (2)	0.047 (13)	2.7

**Table V.** Fractional Coordinates and Equivalent Isotropic Thermal Parameters for (DBr-DCNQI)<sub>2</sub>Cu (Room-Temperature Structure)

atom	x	y	z	$B_{\text{eq}}, \text{\AA}^2$
Cu	0	0.25	0.125	2.0
N(1)	0.4271 (3)	0.2860 (3)	-0.3923 (18)	2.3
N(2)	0.3266 (2)	0.3200 (3)	-0.1652 (17)	2.1
C(1)	0.2908 (3)	0.2856 (3)	0.0365 (17)	1.7
C(2)	0.3061 (3)	0.2235 (3)	0.1463 (18)	1.7
C(3)	0.2670 (3)	0.1899 (3)	0.3422 (18)	1.7
C(4)	0.3798 (3)	0.2988 (3)	-0.2744 (18)	1.7
BR	0.2899 (0)	0.1092 (0)	0.4744 (2)	2.6
H(1)	0.354 (3)	0.206 (4)	0.087 (22)	2.9

**Table VI.** Fractional Coordinates and Equivalent Isotropic Thermal Parameters for (MeCl-DCNQI)<sub>2</sub>Cu (Room-Temperature Structure)

atom	x	y	z	$B_{\text{eq}}, \text{\AA}^2$
Cu	0	0.25	0.125	1.9
N(1)	0.4273 (2)	0.2863 (2)	-0.3925 (12)	2.4
N(2)	0.3273 (2)	0.3213 (2)	-0.1527 (12)	2.2
C(1)	0.2911 (2)	0.2855 (2)	0.0451 (12)	1.9
C(2)	0.3053 (2)	0.2228 (2)	0.1392 (12)	2.1
C(3)	0.2668 (2)	0.1881 (2)	0.3312 (12)	1.9
C(4)	0.2840 (1)	0.1159 (1)	0.4342 (7)	3.2
C(5)	0.3799 (2)	0.2997 (2)	-0.2718 (14)	2.0
H(1)	0.341 (2)	0.204 (2)	0.044 (16)	1.4
H(2)	0.313 (6)	0.102 (6)	0.362 (37)	3.0
H(3)	0.247 (6)	0.089 (5)	0.404 (36)	3.0
H(4)	0.304 (6)	0.115 (6)	0.585 (42)	3.0

**Table VII.** Fractional Coordinates and Equivalent Isotropic Thermal Parameters for (BrCl-DCNQI)<sub>2</sub>Cu (Room-Temperature Structure)

atom	x	y	z	$B_{\text{eq}}, \text{\AA}^2$
Cu	0	0.25	0.125	1.6
N(1)	0.4278 (3)	0.2870 (3)	-0.3936 (19)	2.4
N(2)	0.3267 (3)	0.3203 (2)	-0.1632 (18)	2.1
C(1)	0.2907 (3)	0.2849 (3)	0.0390 (17)	1.5
C(2)	0.3057 (3)	0.2233 (3)	0.1401 (19)	1.8
C(3)	0.2679 (3)	0.1900 (3)	0.3451 (20)	1.9
C(4)	0.3793 (3)	0.2989 (3)	-0.2793 (20)	1.7
BR	0.2881 (1)	0.1110 (1)	0.4602 (4)	3.0

was confirmed by the low-temperature X-ray diffraction study and XPS.<sup>10</sup> ESR study has indicated that the unpaired electrons residing on Cu ions antiferromagnetically interact through the organic  $\pi$  system.<sup>11</sup> All these solid-state properties can be understood systematically through a consideration of the electronic structure based on the tight-binding band calculations. The fertile solid-state chemistry of the Cu-DCNQI system is the subject of this report.

## Results

**Room-Temperature Crystal Structures. DCNQI Column.** Seven copper salts have been subjected to single-crystal X-ray studies

(11) (a) Werner, H.-P.; von Schütz, J. U.; Wolf, H. C.; Kremer, R.; Gehrke, M.; Aumüller, A.; Erk, P.; Hünig, S. *Solid State Commun.* **1988**, *65*, 809–813. (b) Mori, T.; Inokuchi, H.; Kobayashi, A.; Kato, R.; Kobayashi, H. *Phys. Rev. B* **1988**, *B38*, 5913–5923. (c) Mori, T.; Bandow, S.; Inokuchi, H.; Kobayashi, A.; Kato, R.; Kobayashi, H. *Solid State Commun.* **1988**, *67*, 565–568.

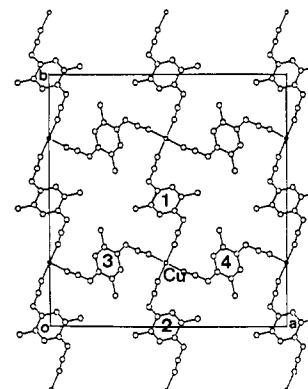
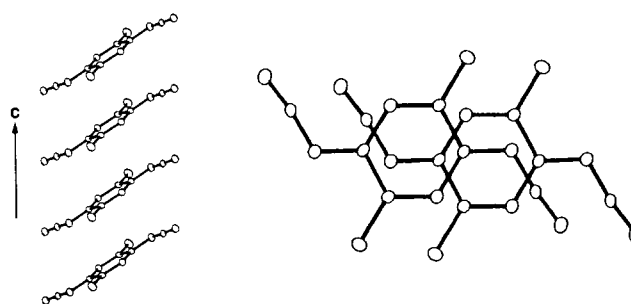
**Table VIII.** Fractional Coordinates and Equivalent Isotropic Thermal Parameters for (DCI-DCNQI)<sub>2</sub>Cu (Room-Temperature Structure)

atom	x	y	z	$B_{\text{eq}}, \text{\AA}^2$
Cu	0	0.25	0.125	2.0
N(1)	0.4271 (2)	0.2874 (2)	-0.3947 (15)	2.5
N(2)	0.3269 (2)	0.3211 (2)	-0.1634 (14)	2.3
C(1)	0.2911 (2)	0.2860 (3)	0.0399 (15)	2.1
C(2)	0.3061 (2)	0.2236 (3)	0.1386 (15)	2.1
C(3)	0.2671 (2)	0.1893 (2)	0.3361 (14)	1.8
C(4)	0.3796 (2)	0.2998 (2)	-0.2773 (16)	2.0
CL	0.2686 (1)	0.1138 (1)	0.4507 (4)	2.7
H(1)	0.347 (3)	0.209 (3)	0.078 (21)	2.8

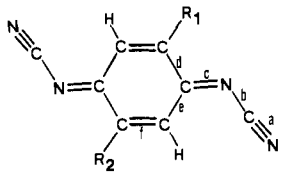
**Table IX.** Interplanar Distances ( $\text{\AA}$ ) of the DCNQI Column in (2,5-R<sub>1</sub>,R<sub>2</sub>-DCNQI)<sub>2</sub>Cu

R <sub>1</sub>	R <sub>2</sub>	interplanar dist	
		RT <sup>a</sup>	100 K
Me	Me	3.214	3.161
MeO	MeO	3.206	
Me	Br	3.180	3.114
Br	Br	3.193	
Me	Cl	3.183	3.110
Br	Cl	3.129	3.108
Cl	Cl	3.159	

<sup>a</sup>RT, room temperature.

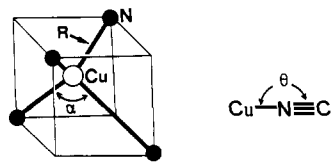
**Figure 2.** Room-temperature (DMe-DCNQI)<sub>2</sub>Cu structure viewed down the *c* axis showing the molecule number scheme used in Table XVII.**Figure 3.** (a, left) Face-to-face stacking of DMe-DCNQI molecules in the room-temperature (DMe-DCNQI)<sub>2</sub>Cu structure. (b, right) Mode of overlapping.

at room temperature. Crystal data are summarized in Table I. Final fractional coordinates and isotropic thermal parameters are given in Tables II–VIII. All these seven Cu salts are isomorphous with space group *I*4<sub>1</sub>/*a* (Figure 2). The DCNQI molecules are uniformly arranged in the one-dimensional column. Stacking is along the crystallographic *c* axis, which corresponds to the longest crystal dimension (Figure 3). The interplanar distances between least-squares planes through the six-membered rings of the DCNQI units are in the range of 3.13–3.21  $\text{\AA}$  (Table IX), which are comparable to those in uniform TCNQ columns. The overlap of the DCNQI molecules within a stack is of the usual “double

Table X. Principal Bond Lengths (Å) and Angles (deg) of 2,5-R<sub>1</sub>,R<sub>2</sub>-DCNQI Molecules


R <sub>1</sub>	R <sub>2</sub>	a	b	c	d	e	f	∠N-C-N	∠C-N-C	
Me	Me	1.159 (6)	1.312 (6)	1.342 (6)	1.433 (6)	1.442 (6)	1.350 (6)	172.8 (5)	119.8 (4)	RT <sup>a</sup>
MeO	MeO	1.150 (8)	1.321 (7)	1.335 (7)	1.452 (8)	1.413 (8)	1.352 (8)	171.2 (7)	120.4 (5)	RT
Me	Br	1.162 (5)	1.296 (5)	1.329 (5)	1.449 (5)	1.428 (5)	1.342 (5)	172.4 (4)	120.3 (4)	RT
Br	Br	1.152 (9)	1.306 (8)	1.329 (9)	1.434 (9)	1.443 (9)	1.350 (9)	172.4 (7)	120.6 (6)	RT
Me	Cl	1.159 (6)	1.309 (6)	1.335 (6)	1.454 (6)	1.436 (7)	1.339 (6)	173.1 (5)	119.9 (4)	RT
Br	Cl	1.163 (9)	1.304 (9)	1.336 (9)	1.446 (9)	1.422 (9)	1.342 (10)	171.9 (7)	120.1 (6)	RT
Cl	Cl	1.150 (7)	1.299 (7)	1.330 (7)	1.443 (7)	1.433 (8)	1.351 (7)	172.4 (6)	120.1 (5)	RT
Me	Me	1.159 (2)	1.311 (2)	1.334 (2)	1.441 (2)	1.435 (2)	1.362 (2)	173.2 (2)	120.0 (1)	100 K
Me	Br	1.172 (5)	1.301 (5)	1.335 (5)	1.453 (5)	1.426 (5)	1.358 (5)	173.1 (4)	120.1 (3)	100 K
Br	Cl	1.163 (10)	1.328 (9)	1.331 (9)	1.446 (9)	1.466 (9)	1.357 (9)	172.6 (7)	120.1 (6)	100 K
Me	Cl	1.170 (8)	1.313 (8)	1.336 (8)	1.446 (9)	1.437 (8)	1.349 (9)	173.2 (6)	120.0 (5)	100 K
H	H	1.150 (2)	1.334 (2)	1.303 (2)	1.446 (2)	1.450 (2)	1.336 (2)	172.8 (2)	119.5 (2)	neutral <sup>b</sup>
Me	Me	1.145 (3)	1.328 (3)	1.323 (3)	1.451 (3)	1.436 (3)	1.350 (3)	172.8 (2)	119.5 (2)	Li salt <sup>c</sup>

<sup>a</sup>RT, room temperature. <sup>b</sup>Reference 12. <sup>c</sup>Reference 13.

Table XI. Metal-Insulator Transition Temperature ( $T_{M-I}$ ) and Coordination Geometry of Cu


R <sub>1</sub>	R <sub>2</sub>	$T_{M-I}$ , <sup>a</sup> K	R, Å		$\alpha$ , deg		$\Delta\alpha$ , <sup>c</sup> deg	$\theta$ , deg	
			RT <sup>b</sup>	100 K	RT	100 K		RT	100 K
Me	Me	metal	1.976 (4)	1.969 (2)	124.5 (2)	126.0 (1)	1.5	170.6 (4)	169.0 (2)
MeO	MeO	metal	1.988 (5)		126.0 (2)			177.6 (5)	
Me	Br	152° 156 <sup>X</sup>	1.979 (2)	1.958 (3)	125.3 (1)	128.2 (1)	2.9	168.6 (2)	168.2 (3)
Br	Br	161° 160 <sup>X</sup>	1.973 (7)		125.3 (3)			169.2 (6)	
Me	Cl	210° 210 <sup>X</sup>	1.964 (4)	1.944 (6)	126.2 (2)	129.1 (3)	2.9	169.7 (4)	169.4 (5)
Br	Cl	213° 210 <sup>X</sup>	1.963 (7)	1.957 (7)	126.1 (3)	129.1 (3)	3.0	167.0 (6)	166.6 (6)
Cl	Cl	230°	1.972 (5)		127.1 (2)			168.1 (4)	

<sup>a</sup>The superscripts c and X indicate  $T_{M-I}$  determined by resistivity measurements<sup>8c</sup> and the abrupt lattice distortion detected from X-ray experiments, respectively. <sup>b</sup>RT, room temperature. <sup>c</sup> $\alpha(100\text{ K}) - \alpha(\text{RT})$ .

bond over ring" type, commonly observed in the anion-radical salts of TCNQs (Figure 3).

**DCNQI Molecule.** Each DCNQI unit is situated on a crystallographic center of inversion. Thus, in the case of asymmetric DCNQI ( $R_1 \neq R_2$ ) salts, there is an orientational disorder. X-ray diffuse scattering observed on the oscillation photographs around the  $c$  axis suggests that the orientation is not completely random. Along the  $c$  axis, the asymmetric DCNQI molecules seem to exhibit short-range ordering with alternate orientation. The principal bond lengths and angles in the DCNQI molecule are given in Table X. They are compared with those in the neutral unsubstituted DCNQI<sup>12</sup> and in the isostructural lithium salts where the formal charge of the DCNQI is  $-1/2$ .<sup>13</sup> The bond length variations associated with the formal charge can be explained on the basis of the coefficients of the LUMO of the neutral molecule. The most significant variations are observed in the bond lengths  $b$  and  $c$ . The transformation from the neutral molecule to the anion shortens the bonding  $b$  and lengthens the anti-bonding  $c$ . The relations of  $b > c$  in the neutral molecule is still kept in the Li salts but turns  $b < c$  in all the Cu salts. This suggests the notion of more than one-half unit negative charge per DCNQI unit in the Cu salts. Further evidences for the degree of charge transfer

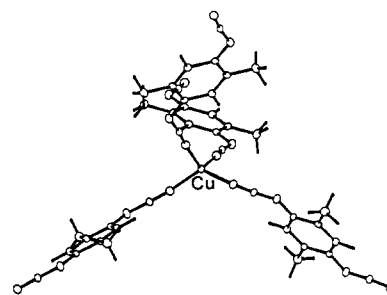


Figure 4. Distorted tetrahedral coordination around Cu in the room-temperature (DMe-DCNQI)<sub>2</sub>Cu structure.

were obtained from the low-temperature X-ray diffraction experiments (vide infra) and XPS measurements.<sup>10</sup> The central six-membered ring is planar in each case, and the  $N$ -cyano groups exhibit slight deviations (0.009–0.066 Å) from the plane defined by the central six-membered ring.

**Coordination Geometry of Cu.** The Cu cation on the  $\bar{4}$  axis is coordinated in  $D_{2d}$  distorted tetrahedral fashion to the N atoms of the  $N$ -cyano groups in the DCNQI molecule (Figure 4). The significant coordination parameters ( $R$ ,  $\alpha$ , and  $\theta$ ) are listed in Table XI. The Cu–N distances ( $R$ ) are comparable to those in the tetrahedral complex [Cu(CH<sub>3</sub>CN)<sub>4</sub>]ClO<sub>4</sub> (1.95–2.02 Å).<sup>14</sup>

(12) Andreetti, G. D.; Bradamante, S.; Bizzarri, P. C.; Pagani, G. A. *Mol. Cryst. Liq. Cryst.* **1985**, *120*, 309–314.

(13) (a) Kato, R.; Kobayashi, H.; Kobayashi, A.; Mori, T.; Inokuchi, H. *Chem. Lett.* **1987**, 1579–1582. (b) Kato, R.; Kobayashi, H.; Kobayashi, A.; Mori, T.; Inokuchi, H. *Synth. Met.* **1988**, *27*, B263–B268.

(14) Csöregy, I.; Kierkegaard, P.; Norrestam, R. *Acta Crystallogr.* **1975**, *B31*, 314–317.

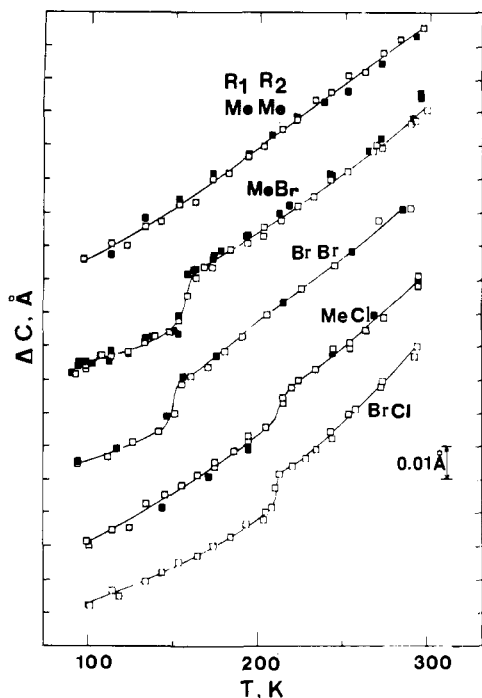


Figure 5. Temperature dependence of the crystallographic  $c$  axis for a series of  $(2,5-R_1,R_2\text{-DCNQI})_2\text{Cu}$ .

The N–Cu–N angles ( $\alpha$ ) indicate the degree of distortion from the  $T_d$  symmetry, ranging from 124.5 to 127.1°. The Cu–N–C angles ( $\theta$ ) fall within the range 167.0–170.6°, except for that in  $(\text{DMeO-DCNQI})_2\text{Cu}$  ( $R_1 = R_2 = \text{MeO}$ ; 177.6°). This distinctive  $\theta$  value in  $(\text{DMeO-DCNQI})_2\text{Cu}$  is probably due to the larger size of the methoxy group. A difference in the  $\theta$  value means a difference in the metal–ligand orbital overlapping. These coordination parameters play an important role in an explanation of the electronic structure (vide infra).

**Temperature Dependences of the Lattice Constants.** The lattice constants were measured down to 100 K. In every case, the lattice constant  $a$  shows a negative thermal expansion. On the other hand, the thermal expansion of  $c$  is normal.<sup>8a,10</sup> The lattice constants of the metallic  $(\text{DMe-DCNQI})_2\text{Cu}$  show no anomaly throughout the entire range of temperatures investigated.<sup>10</sup> The other four salts clearly exhibit an abrupt decrease in  $c$  at the metal–insulator transition temperature  $T_{M-1}$  (Figure 5). Although the accuracy is not enough, an abrupt increase in  $a$  is also observed at  $T_{M-1}$ .<sup>8a,10</sup> The magnitude of the decrease in  $c$  at  $T_{M-1}$  seems to become large with lowering  $T_{M-1}$ . These results indicate that the metal–insulator transition in the Cu–DCNQI system involves a structural transition.

**Low-Temperature Crystal Structures.** The oscillation photographs around the  $c$  axis (the stacking axis) of  $(\text{MeCl-DCNQI})_2\text{Cu}$  were taken at 298 and 100 K. The photograph at 100 K clearly shows the appearance of new reflections indicating the 3-fold superstructure.<sup>9</sup> The same experiment for  $(\text{MeBr-DCNQI})_2\text{Cu}$  also indicated the periodic lattice distortion with a period of  $3c$ . The superstructure wave vector  $(0,0,c^*/3)$  ( $c^*$  is the reciprocal lattice vector) was further confirmed by examining the profile of a satellite reflection  $(4a^*, 8b^*, (2-0.33)c^*)$  at 98 K with use of the X-ray diffractometer (Figure 6). Figure 7 shows that the satellite reflections develop discontinuously at  $T_{M-1}$ . X-ray oscillation photographs were taken also for metallic  $(\text{DMe-DCNQI})_2\text{Cu}$  at 103 K, and only strong diffuse scattering probably due to normal lattice vibrations was observed. All these findings suggest that the metal–insulator transition is a kind of CDW transition. From the viewpoint of the CDW transition, the 3-fold superstructure implies that the formal charge of the DCNQI unit is  $-2/3$  and the valency of Cu is  $+4/3$ , that is, mixed valent between

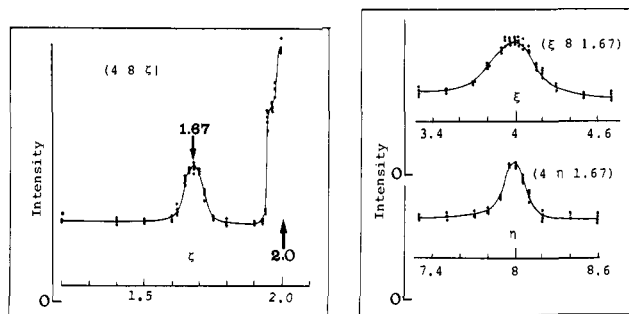


Figure 6. X-ray diffraction profiles at  $(4a^*, 8b^*, (2-0.33)c^*)$  for  $(\text{MeBr-DCNQI})_2\text{Cu}$ , scanned along the  $a^*$ ,  $b^*$ , and  $c^*$  directions, respectively.

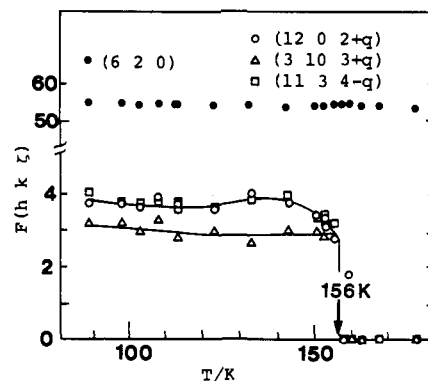


Figure 7. Temperature dependence of the satellite peak intensities in  $(\text{MeBr-DCNQI})_2\text{Cu}$ , where  $q$  is 0.33. A normal Bragg reflection  $(6, 2, 0)$  is inserted for comparison.

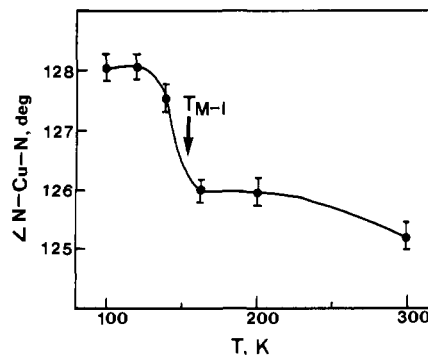


Figure 8. Temperature dependence of  $\alpha$  ( $\angle\text{N-Cu-N}$ ) in  $(\text{MeBr-DCNQI})_2\text{Cu}$ .

+1 and +2 ( $\text{Cu}^+:\text{Cu}^{2+} = 2:1$ ). The formal charge  $-1/3$  per DCNQI (thus,  $\text{Cu}^+:\text{Cu}^0 = 2:1$ ) is also consistent with the 3-fold superstructure. However, this possibility is not plausible, considering the results of XPS<sup>10</sup> and the bond length examination of DCNQI. The absence of the diffuse streaks suggests that the one-dimensional lattice softening (the Kohn anomaly) is not strong in  $(\text{DMe-DCNQI})_2\text{Cu}$ .<sup>10</sup>

The average crystal structures of the low-temperature insulator phase were determined at 100 K for  $(\text{MeCl-DCNQI})_2\text{Cu}$ ,  $(\text{MeBr-DCNQI})_2\text{Cu}$ , and  $(\text{BrCl-DCNQI})_2\text{Cu}$ . The 100 K structure of the metallic  $(\text{DMe-DCNQI})_2\text{Cu}$  was also determined. The crystal data are summarized in Table XII. The final positional parameters are listed in Tables XIII–XVI. The interplanar spacings in the DCNQI columns are slightly reduced from the corresponding room-temperature values (Table IX). Around the Cu cation, the Cu–N distances are slightly shortened and the Cu–N–C angles ( $\theta$ ) remain unchanged. The N–Cu–N angles ( $\alpha$ ), however, exhibit significant change (Table XI). The  $\Delta\alpha$  [ $\alpha(100\text{ K}) - \alpha(\text{RT})$ , Table XI] values clearly distinguish the metallic  $(\text{DMe-DCNQI})_2\text{Cu}$  from the other insulating salts. We have examined the  $\alpha$  value of  $(\text{MeBr-DCNQI})_2\text{Cu}$  at six points of

(15) Bourbonnais, C.; Wzietek, P.; Jerome, D.; Valade, L.; Cassoux, P. *Europhys. Lett.* **1988**, *6*, 177–182.

Table XII. Summary of Crystal Data (at 100 K)

compound	(DMe-DCNQI) <sub>2</sub> Cu	(MeBr-DCNQI) <sub>2</sub> Cu	(MeCl-DCNQI) <sub>2</sub> Cu	(BrCl-DCNQI) <sub>2</sub> Cu
formula	C <sub>20</sub> H <sub>16</sub> N <sub>8</sub> Cu	C <sub>18</sub> H <sub>10</sub> N <sub>8</sub> Br <sub>2</sub> Cu	C <sub>18</sub> H <sub>10</sub> N <sub>8</sub> Cl <sub>2</sub> Cu	C <sub>16</sub> H <sub>4</sub> N <sub>8</sub> Br <sub>2</sub> Cl <sub>2</sub> Cu
crystal dimens, mm	0.22 × 0.18 × 0.35	0.15 × 0.15 × 0.20	0.20 × 0.15 × 0.33	0.06 × 0.04 × 0.25
space group	I4 <sub>1</sub> /a	I4 <sub>1</sub> /a <sup>a</sup>	I4 <sub>1</sub> /a <sup>a</sup>	I4 <sub>1</sub> /a <sup>a</sup>
cell dimens				
a, Å	21.566 (5)	21.627 (10)	21.640 (7)	21.683 (12)
c, Å	3.801 (1)	3.780 (2)	3.745 (2)	3.783 (1)
V, Å <sup>3</sup>	1767.6	1768.0	1753.7	1778.4
Z	4	4	4	4
d <sub>calcd</sub> , g/cm <sup>3</sup>	1.623	2.110	1.791	2.250
linear absorpn coeff, cm <sup>-1</sup>	12.62	57.40	15.79	60.09
scan width (Δω), deg	1.31 + 0.5 tan θ	1.67 + 0.5 tan θ	1.52 + 0.5 tan θ	1.16 + 0.5 tan θ
scan speed, deg/min	4.0	4.0	4.0	4.0
2θ range, deg	3–55	0–60	0–50	4–60
total no. of obsd reflctns	1237	1581	1235	1566
no. of unique data with  F <sub>o</sub>   > 3σ( F <sub>o</sub>  )	937	1122	877	932
weighting scheme <sup>b</sup>	b = 0.01	b = 0.01	b = 0.003	b = 0.1
R	0.0264	0.0480	0.0839	0.0638
R <sub>w</sub>	0.0429	0.0848	0.1196	0.1209

<sup>a</sup> For average structure. The 3-fold satellite reflections that were extremely weak were neglected. <sup>b</sup>  $w = 1/(10.0 + b|F_o|^2)$  ( $|F_o| < 15.0$ ),  $w = 1/(\sigma^2(F_o) + b|F_o|^2)$  ( $|F_o| \geq 15.0$ ).

Table XIII. Fractional Coordinates and Equivalent Isotropic Thermal Parameters for (DMe-DCNQI)<sub>2</sub>Cu (at 100 K)

atom	x	y	z	B <sub>eq</sub> , Å <sup>2</sup>
Cu	0	0.25	0.125	0.7
N(1)	0.4274 (1)	0.2867 (1)	-0.3896 (4)	1.0
N(2)	0.3270 (1)	0.3219 (1)	-0.1519 (4)	0.9
C(1)	0.2904 (1)	0.2862 (1)	0.0449 (4)	0.8
C(2)	0.3056 (1)	0.2235 (1)	0.1368 (4)	0.9
C(3)	0.2671 (1)	0.1874 (1)	0.3338 (4)	0.8
C(4)	0.2825 (1)	0.1213 (1)	0.4210 (5)	1.1
C(5)	0.3797 (1)	0.3001 (1)	-0.2718 (4)	0.9
H(1)	0.342 (1)	0.207 (1)	0.047 (7)	2.3
H(2)	0.316 (1)	0.105 (1)	0.297 (8)	3.2
H(3)	0.252 (1)	0.093 (1)	0.351 (7)	2.4
H(4)	0.287 (1)	0.115 (1)	0.648 (7)	3.2

Table XIV. Fractional Coordinates and Equivalent Isotropic Thermal Parameters for (MeBr-DCNQI)<sub>2</sub>Cu (at 100 K)

atom	x	y	z	B <sub>eq</sub> , Å <sup>2</sup>
Cu	0	0.25	0.125	0.8
N(1)	0.4274 (1)	0.2869 (1)	-0.3989 (10)	1.4
N(2)	0.3264 (1)	0.3208 (1)	-0.1651 (9)	1.1
C(1)	0.2906 (2)	0.2852 (2)	0.0384 (10)	0.9
C(2)	0.3056 (1)	0.2234 (2)	0.1374 (9)	0.8
C(3)	0.2674 (1)	0.1883 (2)	0.3400 (9)	0.8
MR	0.2880 (0)	0.1096 (0)	0.4600 (2)	1.2
C(5)	0.3788 (2)	0.2977 (2)	-0.2837 (10)	0.9
H(1)	0.338 (2)	0.194 (2)	0.028 (15)	1.2

Table XV. Fractional Coordinates and Equivalent Isotropic Thermal Parameters for (MeCl-DCNQI)<sub>2</sub>Cu (at 100 K)

atom	x	y	z	B <sub>eq</sub> , Å <sup>2</sup>
Cu	0	0.25	0.125	0.7
N(1)	0.4277 (3)	0.2868 (2)	-0.4019 (14)	1.2
N(2)	0.3268 (2)	0.3219 (2)	-0.1630 (13)	0.9
C(1)	0.2903 (3)	0.2863 (3)	0.0386 (14)	0.8
C(2)	0.3055 (3)	0.2239 (3)	0.1355 (15)	1.0
C(3)	0.2674 (3)	0.1884 (3)	0.3338 (15)	1.0
C(4)	0.3797 (3)	0.3003 (3)	-0.2810 (16)	0.8
ML	0.2852 (1)	0.1162 (1)	0.4421 (6)	1.3
H(1)	0.353 (4)	0.203 (4)	0.053 (24)	1.4
H(2)	0.328 (9)	0.102 (8)	0.362 (53)	2.9
H(3)	0.236 (8)	0.084 (8)	0.324 (57)	2.9
H(4)	0.323 (8)	0.112 (9)	0.604 (58)	2.9

temperature from 299 K down to 100 K. In order to exclude the systematic error, data collections were performed successively with the same crystal. Figure 8 clearly indicates that the deformation of the coordination tetrahedron occurs intensively at  $T_{M-1}$ , which corresponds to the nature of the discontinuous change observed in the lattice constants at  $T_{M-1}$ .

Table XVI. Fractional Coordinates and Equivalent Isotropic Thermal Parameters for (BrCl-DCNQI)<sub>2</sub>Cu (at 100 K)

atom	x	y	z	B <sub>eq</sub> , Å <sup>2</sup>
Cu	0	0.25	0.125	0.7
N(1)	0.4280 (3)	0.2882 (3)	-0.4026 (20)	1.3
N(2)	0.3258 (3)	0.3213 (3)	-0.1731 (17)	0.8
C(1)	0.2904 (3)	0.2862 (3)	0.0319 (19)	0.7
C(2)	0.3062 (3)	0.2232 (3)	0.1397 (17)	0.8
C(3)	0.2674 (3)	0.1891 (3)	0.3422 (18)	0.6
C(4)	0.3796 (3)	0.3002 (3)	-0.2890 (20)	0.8
BR	0.2890 (0)	0.1109 (0)	0.4636 (3)	1.3

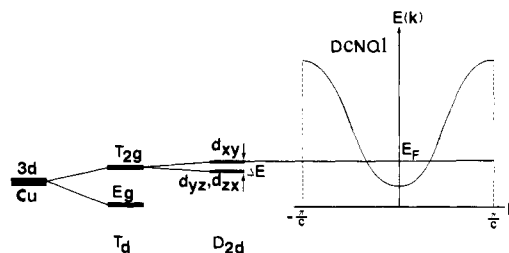


Figure 9. Qualitative interaction diagram depicting the interaction between the d orbitals of Cu and the organic one-dimensional band.

The metal-insulator transition in the Cu-DCNQI system can be described as a cooperative structural-phase transition induced by the CDW instability of the DCNQI column and the intensive deformation of the coordination tetrahedron around the Cu cation.

## Discussion

The electrical properties are sensitive to the substituents R<sub>1</sub> and R<sub>2</sub>. The structural feature of the DCNQI column is almost common to all the Cu salts, while there are small but significant differences in the coordination geometry around the Cu cation. The observation of the metal-insulator transition associated with the CDW formation along the *c* axis strongly suggests the one-dimensional character which arises from the DCNQI column. The conduction path in the Cu-DCNQI system is considered to be formed mainly by overlapping of the LUMOs of the DCNQI molecule. The mixed-valent state of the Cu cation means that the high-lying 3d orbitals are located near the Fermi level of the one-dimensional  $\pi\pi$  band (Figure 9). In the ideal  $T_d$  crystal field, the high-lying d orbitals are the  $d_{xy}$ ,  $d_{yz}$ , and  $d_{xz}$  ( $T_{2g}$ ) orbitals. The  $D_{2d}$  distortion of the coordination tetrahedron removes the degeneracy of the  $T_{2g}$  orbitals, leaving the higher  $d_{xy}$  level and the lower doubly degenerated  $d_{yz}$  ( $d_{xz}$ ) level. We, therefore, consider the electronic structure near the Fermi level based on the DCNQI's LUMO, and three atomic d orbitals ( $d_{xy}$ ,  $d_{yz}$ , and  $d_{xz}$ ) in Cu. In order to examine the effect of the  $\pi\pi$ -d mixing on the original one-dimensional  $\pi\pi$  band, we first calculated the

**Table XVII.** Intermolecular Overlap Integrals among the LUMOs of DCNQi and the d Orbitals of Cu

Cu	DCNQi <sup>a</sup>	(DMe-DCNQi) <sub>2</sub> Cu (×10 <sup>-3</sup> )	(DMeO-DCNQi) <sub>2</sub> Cu (×10 <sup>-3</sup> )
d <sub>xy</sub> .....	1	4.82	3.48
	2	4.82	3.48
	3	4.82	3.48
	4	4.82	3.48
d <sub>yz</sub> .....	1	0.47	1.77
	2	-0.47	-1.77
	3	3.47	4.15
	4	-3.47	-4.15
d <sub>xz</sub> .....	1	3.47	4.15
	2	-3.47	-4.15
	3	-0.47	-1.77
	4	0.47	1.77
DCNQi...DCNQi (in column)		16.65	16.04

<sup>a</sup>The molecule number scheme is shown in Figure 2.

overlap integrals ( $S$ ) among these conduction orbitals in (DMe-DCNQi)<sub>2</sub>Cu. The LUMO of the DCNQi molecule was calculated with the extended Hückel method. The results are listed in Table XVII. The strongest interaction is observed along the DCNQi column, which confirms the notion that the main conduction path is along the DCNQi column. The interactions between the LUMO and the d orbitals are small but significant.

In the next step, we have carried out tight-binding band electronic structure calculations with use of the approximation that the transfer integral ( $t$ ) is proportional to the overlap integral ( $t = \epsilon S$ , where  $\epsilon$  is a constant of the order of the energy of the LUMO). For the calculations, the tetragonal body-centered lattice ( $a_0, b_0, c_0$ ) is reduced to the following primitive cell;  $a = a_0$ ,  $b = (a_0 + b_0 + c_0)/2$ ,  $c = c_0$ . The unit cell contains four DCNQi units and two Cu cations. If there is no  $p\pi$ -d mixing, the band structure consists of one-dimensional (4-fold degenerate)  $p\pi$  bands and d bands with constant energy level. The Fermi surface contains a pair of flat sheets. Such a purely one-dimensional system will easily undergo the metal-insulator transition associated with the CDW or SDW formation. This may be the case of the DCNQi salts with closed-shell monocations.<sup>16</sup> The  $p\pi$ -d interaction, however, removes the degeneracy of the  $p\pi$  bands to generate a multiple Fermi surface. If there is no single periodical lattice distortion wave that can open the gap all over the Fermi surface, a complete gap formation by the CDW requires a complex distortion of the lattice, which is no longer so energetically favorable. As for the SDW formation, that will also be hindered by the frustration effects due to the mismatch among the several Fermi wave vectors.<sup>15</sup> The system will resist the CDW or SDW formation in this way, in spite of the sheetlike Fermi surface. We call such a stable metallic system a multi-Fermi surface system.

If the  $p\pi$ -d interaction is strong enough, the system will exhibit a three-dimensional character. In this Cu-DCNQi system, however, the  $p\pi$ -d interaction is not so strong as to construct the three-dimensional electronic structure and the d-origin energy bands show rather small dispersion. In the case of such a narrow band, the independent electron approximation will not be adequate and the electrons associated with the d-origin bands will tend to localize on the Cu cations. The localized electrons on the Cu cations do not contribute to the electrical conduction but play an important role in the magnetic properties. The ESR study indicates the antiferromagnetic ordering of the spins on Cu at low temperature.<sup>8,11</sup> Considering the long Cu...Cu distances (ca. 3.9 Å), this magnetic interaction should be mediated by the DCNQi molecule. Of course, we have presented a rough depiction. Because of the  $p\pi$ -d mixing, the d electrons on Cu are not completely localized and exhibit itinerant character. The conduction behavior, however, should be determined mainly by the organic  $p\pi$  system.

The appearance of the multi-Fermi surface character depends on the energy splitting  $\Delta E = E(d_{xy}) - E(d_{xz}, d_{yz})$  (the energy is

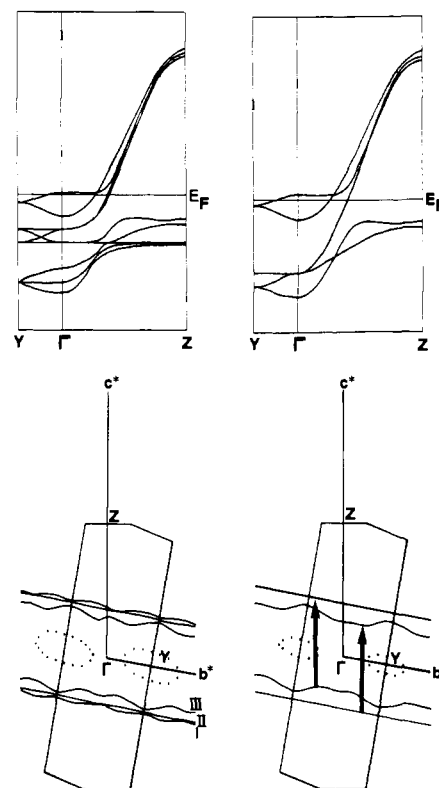


**Figure 10.** Band structure and multiple Fermi surface of (DMe-DCNQi)<sub>2</sub>Cu. (a, left)  $E(d_{xz}, d_{yz}) = 1.5E(d_{xy})$ . (b, right) The  $\Delta E$  value is large enough. See also Figure 9.

measured from the LUMO level hereafter) associated with the distortion of the coordination tetrahedron. In Figure 10a, the band structure in the case of  $E(d_{xz}, d_{yz}) = 1.5E(d_{xy})$  is shown as an example of that in the metallic state. The Fermi surface contains three pairs of sheets (I, II, III). The absence of the particular relation among three Fermi wave vectors indicates that a complete gap formation over these surfaces cannot be accomplished by a single modulation vector. The closed Fermi surface represented by a dotted line in Figure 10 arises mainly from the narrow d band and is considered to be an apparent one. With an increase in the  $\Delta E$  value accompanying the distortion of the coordination tetrahedron, the contribution of the  $d_{xz}$  and  $d_{yz}$  orbitals to the electronic structure near the Fermi level decreases and the sheets I and II come close to each other. When the  $d_{xz}$  and  $d_{yz}$  orbitals are neglected (the  $\Delta E$  value is large enough), the band structure becomes rather simple (Figure 10b). There are six energy branches. Two branches (doubly degenerated) have purely  $p\pi$  character. The Fermi surface associated with these branches contains a pair of completely planar sheets, which can be nested into another pair of sheets with the wave vector  $k_z \approx c^*/3$ . In this case, an energy gap is created over the whole actual Fermi surface. This feature well explains the CDW formation coupled with the intensive deformation of the coordination tetrahedron at  $T_{M-1}$ . It should be noticed that the deformation at  $T_{M-1}$  stabilizes the lower  $d_{xz}$  and  $d_{yz}$  orbitals and the total energy of  $\text{Cu}^{2+}$  ( $d^9$ ) is lowered. The rapid increase in the resistivity at  $T_{M-1}$ , which was not observed in the alkali-metal (or  $\text{NH}_4$ ) salts, implies that the energy gap arises not only from the stabilization of the DCNQi column but also from the stabilization of the  $d^9$  system associated with the deformation of the coordination tetrahedron.<sup>8a</sup> Thus, this metal-insulator transition is not a usual CDW transition, which is consistent with the lack of the one-dimensional precursor diffuse scattering.<sup>16</sup> The above discussion suggests that the smaller room-temperature  $\Delta E$  value means the stronger multi-Fermi surface character and promises the lower metal-insulator transition temperature. We roughly estimated the crystal field splitting of the d orbitals  $\Delta E$  from the Cu-N distance ( $R$ ) and the N-Cu-N angle ( $\alpha$ ) at room temperature. For the copper(II) ion, the

(16) Moret, R. *Synth. Met.* 1988, 27, B301-B307.

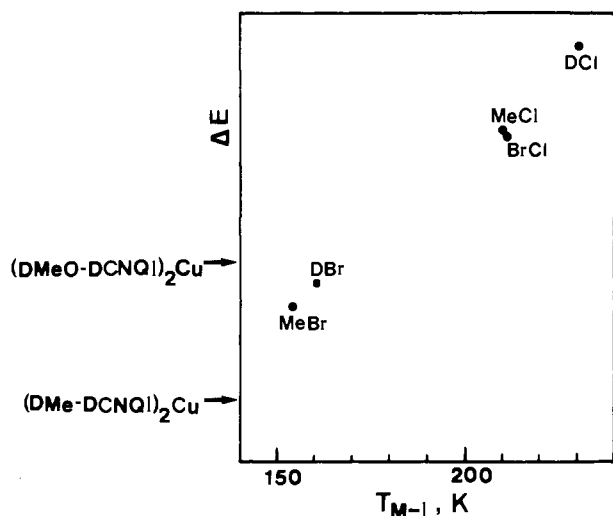


Figure 11. Correlation between the crystal field splitting  $\Delta E$  (arbitrary unit) at room temperature and the metal-insulator transition temperature  $T_{M-1}$ , for  $(2,5-R_1, R_2\text{-DCNQI})_2\text{Cu}$ .  $R_1$  and  $R_2$  for each point are, respectively as follows: MeBr, CH<sub>3</sub> and Br; DBr, Br and Br; MeCl, CH<sub>3</sub> and Cl; BrCl, Br and Cl; DCI, Cl and Cl.

electrostatic energies of the  $d_{xy}$  and  $d_{xz}$  ( $d_{yz}$ ) orbitals under the perturbation of four negative point charges placed at the apices of the  $D_{2d}$  distorted tetrahedron are represented by Hoffmann and Goslar as follows:<sup>17</sup>

$$E(d_{xy}) = -2D_s(3 \cos^2(\alpha/2) - 1) + (9/140)\Delta_T(35 \cos^4(\alpha/2) - 50 \cos^2(\alpha/2) + 19)$$

$$E(d_{xz}, d_{yz}) = D_s(3 \cos^2(\alpha/2) - 1) - (9/70)\Delta_T(35 \cos^4(\alpha/2) - 30 \cos^2(\alpha/2) + 3)$$

where  $\Delta_T = 16855.488q/R^5$  and  $D_s = 0.565932R^2\Delta_T$  ( $q$  is the effective charge of the ligand). Although these expressions contain the electrostatic effects alone, they would make a substantial contribution to the relative  $\Delta E$  values. Since it is difficult to estimate the exact  $q$  value (thus the exact  $\Delta E$  values), we calculated the  $\Delta E/q$  values and plotted them against the transition temperature  $T_{M-1}$ . The metallic  $(\text{DMe-DCNQI})_2\text{Cu}$  gives the smallest  $\Delta E$  value and the plot shows an excellent correlation between the room-temperature  $\Delta E$  and  $T_{M-1}$  (Figure 11).  $(\text{DMeO-DCNQI})_2\text{Cu}$ , however, shows a rather large  $\Delta E$  value, in spite of its stable metallic behavior.

The exceptional behavior of  $(\text{DMeO-DCNQI})_2\text{Cu}$  has led us to notice another factor of the appearance of the multi-Fermi surface character. This is the overlap integrals ( $S$ ) between the LUMO and the d orbitals. We should recall that the Cu-N-C angle ( $\theta$ ) in  $(\text{DMeO-DCNQI})_2\text{Cu}$  is distinct from those in the other six salts, probably due to the larger size of the methoxy groups. Indeed, the calculated  $S$  values for  $(\text{DMeO-DCNQI})_2\text{Cu}$  are clearly different from those for  $(\text{DMe-DCNQI})_2\text{Cu}$  (Table XVII). Figure 12 shows the multiple Fermi surface in  $(\text{DMeO-DCNQI})_2\text{Cu}$  with  $E(d_{xz}, d_{yz}) = 1.5E(d_{xy})$  (the same condition for Figure 10a). Compared with the case of  $(\text{DMe-DCNQI})_2\text{Cu}$  (Figure 10a), the sheets I and II are well separated from each other. It should be reminded that the metal-insulator transition occurs when the sheets I and II are merged into one by the increase of the  $\Delta E$  value. Therefore, the system with better separation of the sheets I and II exhibits the more stable metallic state. Since the  $\Delta E$  value of  $(\text{DMeO-DCNQI})_2\text{Cu}$  is larger than that of  $(\text{DMe-DCNQI})_2\text{Cu}$ , the actual distance between the sheets I and II is slightly shorter than that depicted in Figure 12. The sheets I and II, however, remain well separated. This is the plausible reason why  $(\text{DMeO-DCNQI})_2\text{Cu}$  retains a metallic state in spite of a rather large  $\Delta E$  value.

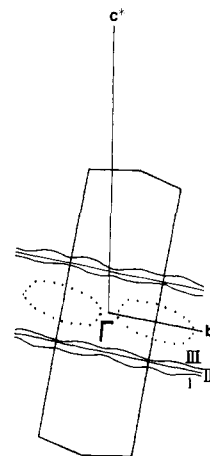


Figure 12. Multiple Fermi surface of  $(\text{DMeO-DCNQI})_2\text{Cu}$ .

We have considered the effects of the crystal field splittings of the d orbitals  $\Delta E$  and the overlap integrals ( $S$ ) between the LUMO and the d orbitals on the multi-Fermi surface nature. The  $\Delta E$  value is a function of the Cu-N distance ( $R$ ) and the N-Cu-N angle ( $\alpha$ ), which are temperature-dependent. On the other hand, the  $S$  value is considered almost independent of the temperature, because the low-temperature crystal structure studies show that the temperature dependence of the Cu-N-Cu angle ( $\theta$ ) is small. The  $S$  value is influenced by the substituents  $R_1$  and  $R_2$ , which is the molecular packing effect. The effect of lowering temperature on the crystal structure will resemble that of the increase in pressure; therefore, the pressure-induced metal-insulator transition observed in  $(\text{DMe-DCNQI})_2\text{Cu}$  and  $(\text{DMeO-DCNQI})_2\text{Cu}$  would be explained by the increase in the  $\Delta E$  value under the high pressure.<sup>9</sup>

Our proposal is that the metallic state in the Cu-DCNQI system is stabilized by its multi-Fermi surface character. We do not adopt other explanations, one of which is the tight crystal packing associated with the Cu-N coordination bonds. This cannot describe the substituent dependence of the stability of the metallic state [for example, the stable metal  $(\text{DMeO-DCNQI})_2\text{Cu}$  has the longest Cu-N distance]. Even if there is a small change of the oxidation state of the Cu cation ( $4/3 \pm \Delta\rho$ ) associated with temperature or pressure, it would not essentially affect the multi-Fermi surface character. The loss of the multi-Fermi surface character is caused by the  $D_{2d}$  distortion of the coordination tetrahedron, which lowers the  $d_{yz}$  and  $d_{xz}$  level far below the Fermi level.

## Conclusion

Among the conducting DCNQI anion-radical salts, the stable metallic state is observed only in the Cu salts. The essential point is the mixed-valence state of the Cu cation, which brings about the  $p\pi$ -d mixing. The  $p\pi$ -d mixing turns the original one-dimensional character associated with the DCNQI chain into the multi-Fermi surface one. This is responsible for the suppression of the metal-insulator transition in  $(\text{DMe-DCNQI})_2\text{Cu}$  and  $(\text{DMeO-DCNQI})_2\text{Cu}$ . In the case of the superconducting BEDT-TTF salts, the two-dimensionality characterized by the closed Fermi surface stabilizes the metallic state. On the other hand, the Fermi surface of the multi-Fermi surface system is sheetlike, and the system preserves the one-dimensional character. The  $D_{2d}$  distortion of the coordination tetrahedron decreases the number of d orbitals participating in the  $p\pi$ -d mixing and weakens the multi-Fermi surface nature, which leads to the gap formation by the CDW. The metal-insulator transition in this system is not the usual simple Peierls type, because the CDW formation occurs in cooperation with the deformation of the coordination tetrahedron. The Cu-DCNQI system contains the  $p\pi$ -origin electrons with the itinerant character and the d-origin electrons associated with the narrow bands. The low-temperature magnetic properties arise mainly from the localized electrons on the Cu cations. The Cu-DCNQI system has provided various problems

(17) Hoffmann, S. K.; Goslar, J. J. *Solid State Chem.* **1982**, *44*, 343-353.



of solid-state chemistry: a new type of electron-phonon coupling (the coupling of the CDW formation and the deformation of the coordination tetrahedron), the pressure-induced metal-insulator transition, the coexistence of the ordered spin structure, and the  $2p\pi$  conduction electrons. Further investigation of the DCNQI system will open up frontiers of the molecular materials.

### Experimental Section

**Starting Materials.** 2,5- $R_1, R_2$ -DCNQIs were synthesized according to the method described in ref 18.  $[\text{Cu}(\text{CH}_3\text{CN})_4]\text{ClO}_4$  was prepared by treating  $\text{Cu}(\text{ClO}_4)_2 \cdot 6\text{H}_2\text{O}$  with Cu granules in refluxing acetonitrile, recrystallized from acetonitrile-ether, and stored under  $\text{N}_2$ . Acetonitrile used for the electrolysis was purified according to mainly ref 19 and stored under  $\text{N}_2$ .

**Crystal Growth.** Single crystals of  $(2,5-R_1, R_2\text{-DCNQI})_2\text{Cu}$  were obtained by the galvanostatic electrolysis of acetonitrile solutions (20 mL) containing 2,5- $R_1, R_2$ -DCNQI (ca.  $7 \times 10^{-3}$  M) and  $[\text{Cu}(\text{CH}_3\text{CN})_4]\text{ClO}_4$  (ca.  $8 \times 10^{-3}$  M). An H-shaped cell was employed. The platinum wire electrodes of 1-mm diameter were soaked in aqua regia and polished by carborundum before use. A nitrogen atmosphere was maintained over the electrolysis solutions. The experimental temperature was in the range of 22–24 °C. A constant current (8–10  $\mu\text{A}$ ) was applied for a period of 4–6 days, after which the black needles formed on the cathode were collected by filtration, washed with acetone and *n*-hexane, and air-dried.

**Crystallographic Studies.** Intensity data at room temperature were recorded on a Rigaku automatic four-circle diffractometer (detector aperture: horizontal, 4.5 mm; vertical, 4.5 mm) using graphite-mo-chromated Mo  $K\alpha$  radiation ( $\lambda = 0.71069 \text{ \AA}$ ) and the  $\omega$ -scan technique. Three standard reflections were monitored every 100 reflections and found to be constant. Background counts of 5 s were taken at each end of the scan. Intensity measurements of weak reflections [ $\sigma(F)/F > 0.1$ ] were repeated up to four times. The intensities were corrected for Lorentz and polarization effects but not for absorption because of the small size of the crystals. Reflections with  $|F_o| < 3\sigma$  were omitted. The refined cell constants from 20 reflections ( $20^\circ < 2\theta < 35^\circ$ ) and additional relevant crystal data are given in Table I.

The structures were solved on the basis of the brief description about the structure of  $(\text{DMe-DCNQI})_2\text{Cu}$  in ref 7 and refined by the block-diagonal least-squares method. Instead of the space group  $I4_1$ , adopted in ref 7,  $I4_1/a$  was taken because an obvious extinction rule of  $h, (k) = 2n$  in  $hk0$  reflections was observed. All calculations were performed on a HITAC M-680H computer at the Computer Centre of the University

of Tokyo, with use of standard programs.<sup>20</sup> Atomic scattering factors and anomalous dispersion terms were taken from ref 21. In the case of the asymmetric DCNQI salts with the orientational disorder, the superimposed atoms were refined with the use of the averaged scattering factors. The agreement factor were defined by  $R = (\sum ||F_o| - |F_c||) / (\sum |F_o|)$ ,  $R_w = [\sum w(|F_o| - |F_c|)^2 / (\sum w|F_o|^2)]^{1/2}$ .

In the low-temperature X-ray studies, sample temperatures were obtained with the use of cold  $\text{N}_2$  stream from liquid  $\text{N}_2$  and a Rigaku variable-temperature controller. The temperature was monitored with a calibrated Cu-constantan thermocouple placed within 3 mm of the sample.

The unit cell parameters were determined as a function of temperature from least-squares analysis of 12 reflections in the range of  $25^\circ < 2\theta < 35^\circ$  automatically centered on the Rigaku four-circle diffractometer. The low-temperature oscillation photographs around the *c* axis were taken on the same diffractometer.

Intensity data were collected at 100 K with the use of the  $\omega$ -scan technique. The same apparatus and method as for the room-temperature measurements were used. The intensities of weak reflections [ $\sigma(F)/F > 0.1$ ] were measured on repeated two or three runs. The intensities of three standard reflections, measured at 100 reflection intervals, were stable throughout the course of data collection. All calculations were performed as for the room-temperature structure.

Data collections for the study of the temperature dependence of  $\alpha$  in  $(\text{MeBr-DCNQI})_2\text{Cu}$  were performed by using the same apparatus and method as for the 100 K measurements.

**Extended Hückel MO Calculations and Tight-Binding Band Calculations.** General procedures have been previously published.<sup>22</sup> The atomic orbitals are simple Slater-type orbitals, but for metallic 3d orbitals we choose two-component orbitals. The exponents and the relative weights for metallic 3d orbitals are taken from ref 23.

**Supplementary Material Available:** Crystal data, atomic parameters, and anisotropic thermal parameters, for  $(\text{MeBr-DCNQI})_2\text{Cu}$  at 299, 200, 163, 149, 120, and 100 K (7 pages); listing of observed and calculated structure factors (54 pages). Ordering information is given on any current masthead page.

(20) UNICS III: Sakurai, T.; Kobayashi, K. *Rep. Inst. Phys. Chem. Res.* **1979**, *55*, 69. ORTEP: Johnson, C. K. ORTEP Report ORNL-3794. Oak Ridge National Laboratory, Oak Ridge, TN, 1965.

(21) *International Tables for X-ray Crystallography*; Kynoch Press: Birmingham, England, 1974; Vol. IV.

(22) Mori, T.; Kobayashi, A.; Sasaki, Y.; Kobayashi, H.; Saito, G.; Inokuchi, H. *Bull. Chem. Soc. Jpn.* **1984**, *57*, 627–633.

(23) Girerd, J. J.; Kahn, O.; Verdager, M. *Inorg. Chem.* **1980**, *19*, 274–276.

(18) Aumüller, A.; Hünig, S. *Liebigs Ann. Chem.* **1986**, 142–164.

(19) Carlsen, L.; Egsgaard, H.; Andersen, J. R. *Anal. Chem.* **1979**, *51*, 1593–1595.